HHS Public Access

Author manuscript

Ann Biomed Eng. Author manuscript; available in PMC 2018 April 01.

Published in final edited form as:

Ann Biomed Eng. 2017 April ; 45(4): 1133–1147. doi:10.1007/s10439-016-1765-5.

Fundamental Principles of Tremor Propagation in the Upper Limb

Andrew D. Davidson[1] and **Steven K. Charles**[1,2]

[1]Department of Mechanical Engineering, Brigham Young University

[2]Neuroscience Center, Brigham Young University

Abstract

Although tremor is the most common movement disorder, there exist few effective tremor-suppressing devices, in part because the characteristics of tremor throughout the upper limb are unknown. To clarify, optimally suppressing tremor requires a knowledge of the mechanical origin, propagation, and distribution of tremor throughout the upper limb. Here we present the first systematic investigation of how tremor propagates between the shoulder, elbow, forearm, and wrist. We simulated tremor propagation using a linear, time-invariant, lumped-parameter model relating joint torques and the resulting joint displacements. The model focused on the seven main degrees of freedom from the shoulder to the wrist and included coupled joint inertia, damping, and stiffness. We deliberately implemented a simple model to focus first on the most basic effects. Simulating tremorogenic joint torque as a sinusoidal input, we used the model to establish fundamental principles describing how input parameters (torque location and frequency) and joint impedance (inertia, damping, and stiffness) affect tremor propagation. We expect that the methods and principles presented here will serve as the groundwork for future refining studies to understand the origin, propagation, and distribution of tremor throughout the upper limb in order to enable the future development of optimal tremor-suppressing devices.

Key Terms

Essential Tremor; Parkinson's Disease; Tremor Suppression; System Dynamics; Frequency Response; Impedance

Introduction

Tremor is the most common movement disorder [2, 19] and results from an interaction between pathological neural control and the frequency response of the limb [23, 29, 30]. The two leading conditions that cause tremor in the upper limb are Essential Tremor and Parkinson's disease. Other conditions that can cause tremor include dystonia, cerebellar ataxia, traumatic brain injury, stroke, and multiple sclerosis [2]. More than 65% of the population with upper limb

Corresponding Author: Steven K. Charles, 435 CTB, Brigham Young University, Provo, UT 84602, skcharles@byu.edu, Phone: 801-422-7369.

Potential Conflict Of Interest: SK Charles is a scientific advisor to, and holds stock in, Vykon Technologies LLC. This company has licensed technology invented by SK Charles to develop markerless monitoring of movement disorders, including tremor.

tremor present serious difficulties performing daily living activities such as eating, buttoning a shirt, writing, etc. [42].

Unfortunately, medication and surgical interventions are only partially effective, and patients have few non-invasive treatment options. For example, the only two medications with unequivocal efficacy in treating Essential Tremor, propranolol (a beta-blocker) and primidone (an anti-convulsant), reduce the tremor by only 50%, and only 50% of patients benefit from one or both of these medications [18, 48]. Patients who do not respond favorably to medication may be eligible for deep brain stimulation (DBS), which provides 55-90% tremor reduction [48] and is effective in 70-90% of patients, though its efficacy is gradually lost in some patients [18]. However, despite its efficacy, DBS is by no means an optimal solution because of its highly invasive nature. Many patients prefer to suffer the debilitating consequences of tremor rather than undergo neurosurgery.

A significant obstacle to developing effective tremor-suppressing devices is that the characteristics of tremor are not known throughout the upper limb. Given the challenges associated with medications and DBS, it is important to give patients non-pharmacological, non-surgical alternatives. Yet there is a surprising lack of effective tremor-suppressing devices. Optimally suppressing tremor requires a knowledge of tremor throughout the upper limb: where in the upper-limb the tremor originates (mechanically), how it propagates, and where it manifests most severely. However, most studies have only investigated tremor in a single degree of freedom (most often either at the endpoint of outstretched arms or in wrist flexion-extension). Therefore, the origin, propagation, and distribution of tremor are currently unknown, greatly limiting our ability to effectively reduce tremor with tremor-suppressing devices.

Tremor propagates because of the mechanics of the limb. Whatever the neural origins may be, at the joint level all types of tremor (pathological or physiological) can be reduced to recurring joint torque that drives the recurring joint motion we call tremor. The amplitude of the tremor depends on the amplitude of the joint torque and the mechanics of the limb. Thus the relationship between torque, limb, and tremor can be thought of as an input (joint torque) that acts on a system (limb), producing an output (tremor). In other words, the limb acts as a filter that attenuates, passes, or amplifies the effect of the joint torque. Therefore, limb mechanics play a significant role in shaping (attenuating, passing, or amplifying) the amplitude of all types of tremor. Note that amplification occurs through resonance, which—depending on the mechanics of the limb and the frequency of the input torque—can occur in (and increase the amplitude of) any type of tremor, be it pathological or physiological. Importantly, limb mechanics not only shape tremor amplitude at the joint where the recurring joint torque acts; because movement in one joint affects movement at other joints through interaction torques, the mechanics of the limb also spread the tremor to other joints, causing the tremor to propagate. Thus tremor propagation is part of the mechanism through which recurring joint torque creates tremor throughout the limb, including clinically relevant endpoint tremor.

The long-term objective of this work is to understand the origin, propagation, and distribution of tremor throughout the upper limb in order to enable the future development of

optimal tremor-suppressing devices. Here we present basic principles underlying the propagation of tremor throughout the upper limb. As this is the first systematic investigation of tremor propagation of which we are aware, we deliberately chose a simple model to focus first on the most basic effects. We simulated tremor propagation using a linear time-invariant (LTI), lumped-parameter model of the relationship between joint torques and the resulting joint displacements. The model included the seven main degrees of freedom (DOF) from the shoulder to the wrist and included coupled joint inertia, damping, and stiffness. We used the model to establish the fundamental principles that govern how tremor source parameters (input torque location and frequency) and joint impedance (inertia, damping, stiffness) affect tremor propagation. Because limb mechanics spread all types of tremor, the principles presented here are relevant to all types of tremor (pathological or physiological).

Methods

Model of Upper Limb Dynamics

Model Development—To establish the most fundamental principles of tremor propagation, we used the arguably simplest possible model between input torques and output displacements that can capture the phenomenon of tremor propagation. A linear model was used because tremor consists of relatively small displacements around an equilibrium point. Prior studies have shown that linear models can effectively capture the key elements of the dynamics of small upper limb movements [3, 39]. In addition, LTI models allow for the use of principles and tools from linear systems theory, including frequency response (see below).

Model Structure—The musculoskeletal dynamics of the upper limb were modeled as $I\ddot{\boldsymbol{q}} + D\dot{\boldsymbol{q}} + K\boldsymbol{q} = \boldsymbol{\tau}$, where $\boldsymbol{q} = [q_1\ q_2\ q_3\ q_4\ q_5\ q_6\ q_7]^T$ represents angular displacement in each DOF, positive in shoulder flexion (q_1), shoulder adduction (q_2), shoulder internal rotation (q_3), elbow flexion (q_4), forearm pronation (q_5), wrist flexion (q_6), and wrist ulnar deviation (q_7) (Figure 1); I, D, and K are 7-by-7 impedance matrices representing the coupled inertia, damping, and stiffness in these DOF, respectively; and $\boldsymbol{\tau} = [\tau_1\ \tau_2\ \tau_3\ \tau_4\ \tau_5\ \tau_6\ \tau_7]^T$ represents the input torque (arising from muscle activity) acting on each DOF.

The diagonal elements of the impedance matrices (I, D, and K) specify the relationship between torque and displacement in the same DOF, whereas the off-diagonal elements represent the relationship between torque and displacement in different DOF. Therefore, the off-diagonal elements specify how the DOF of the upper limb are coupled to each other, which is important to this study since coupling enables tremor propagation. Which off-diagonal elements of the inertia matrix are non-zero (and therefore facilitate coupling) is not easily predicted, so we used software that implemented the iterative Newton-Euler method [8] in conjunction with prior measurements of inertia of individual segments (details below). Stiffness and damping in non-extreme joint postures are due to muscle stretch, and the off-diagonal elements, which couple the DOF, represent multi-articular muscles [26]. Therefore, which off-diagonal elements of the stiffness and damping matrices are non-zero is easily predicted from a knowledge of muscle origin and insertion points. However, some DOF share multi-articular muscles but may experience weak or even negligible coupling, for example because the muscle moment arms are small. We determined the degree of coupling

from prior measurements, if available, or tested a wide variety of plausible values (details below).

Model Parameters—The full 7-by-7 inertia, damping, and stiffness matrices are not available in the literature, so we assembled them from prior studies that measured portions of the matrices (Table 1). Although we estimated values as accurately as possible, the exact values are not critical because we also performed a thorough sensitivity analysis to determine the effect of uncertainty in our values.

Inertia: Prior measurements of inertial values for individual body segments were used in conjunction with the Robotics Vision and Control (RVC) toolbox [6] to calculate the full inertia matrix, including coupling between segments. The RVC toolbox is a toolbox for Matlab (Mathworks, Natick, MA) that is freely available [6] and thoroughly documented [7]. The body-segment inertial parameters were taken from [9] using values for a 50th percentile male. The coupled inertia matrix was calculated for different postures (see below) via Denavit-Hartenberg (DH) parameters [46] using the RVC toolbox, which implemented the iterative Newton-Euler method [8] (Figure 2, Table 2).

Stiffness: We started with purely passive stiffness (no muscle activity) but later added active stiffness to model co-contraction (see below). The diagonal and off-diagonal values corresponding to planar shoulder-elbow movements were taken from the torque-dependent regression by [21], with zero torque for passive stiffness. To estimate the remaining diagonal and off-diagonal elements of the sub-matrix for the shoulder and elbow, we scaled a recent measurement of passive stiffness in the 3 DOF of the shoulder [33] to match the values from [21]. The 3-by-3 sub-matrix representing wrist and forearm stiffness was taken from [16]. The unknown off-diagonal stiffness representing coupling between the shoulder-elbow and the forearm-wrist systems were initially assumed zero but then changed to a variety of non-zero values in the sensitivity analysis. Many studies have shown joint stiffness to be nearly symmetric [16, 26, 38]. To simplify the analysis, we used in our simulations only the symmetric part of the stiffness matrix, calculated as the average of the matrix and its transpose.

Damping: Only few elements of the 7-by-7 damping matrix have been measured. However, several past shoulder-elbow studies have found the shape and orientation of the damping and stiffness ellipses to be similar [15, 41, 47], indicating that the matrices are roughly proportional. Therefore, some past studies involving few DOF have approximated the damping matrix to be proportional to the stiffness matrix, the proportionality constant chosen so the new matrix would match past measurements of individual matrix elements or damping ratios [4, 43]. However, our 7-by-7 matrix involves different sets of multi-articular muscles, and it became clear that a single constant of proportionality was unable to match previously measured damping ratios. Therefore, we used one constant of proportionality (0.07 s) for the 4-by-4 submatrix representing the shoulder-elbow system, and a different constant of proportionality (0.028 s) for the 3-by-3 submatrix representing the forearm-wrist system. The other off-diagonal values are unknown and were initially assumed zero but later varied through a range of nonzero values in the sensitivity analysis. Using two different constants of proportionality allowed shoulder-elbow damping and forearm-wrist damping to be

proportional to shoulder-elbow stiffness and forearm-wrist stiffness, respectively, and for the range of the resulting single-DOF damping ratios (0.18-0.42) to match the range measured previously (0.14-0.48) [22, 31, 41, 45].

Input-Output Relationships—Our model has seven inputs (a torque in each DOF) and seven outputs (a displacement in each DOF). In such a multiple-input–multiple-output model, every input has the potential to affect every output. The relationships between inputs and outputs are given by transfer functions, derived using basic linear systems theory [37] as follows. Our model $I\ddot{\mathbf{q}} + D\dot{\mathbf{q}} + K\mathbf{q} = \boldsymbol{\tau}$ can be transformed into the Laplace domain as $(Is^2 + Ds + K)\mathbf{Q}(s) = \mathbf{T}(s)$, where $\mathbf{Q}$ and $\mathbf{T}$ are the Laplace transforms of $\mathbf{q}$ and $\boldsymbol{\tau}$, respectively, and s is the Laplace variable. Summarizing $Is^2 + Ds + K$ as $Z(s)$ and solving for $\mathbf{Q}$ yields $\mathbf{Q} = Z^{-1}\mathbf{T}$. Defining the transfer function matrix $G(s)$ as Z^{-1} yields $\mathbf{Q} = G\mathbf{T}$. G is a 7-by-7 matrix with 49 transfer functions, one for each input-output relationship, i.e. $Q_{i/k} = G_{ik}T_k$, where $Q_{i/k}$ is the output in DOF i due to an input in DOF k. Each transfer function has the same 14th order denominator, but generally different numerators. The total output at each DOF is a linear combination of the inputs at each DOF, the weights of the linear combination being the transfer functions associated with that output: $Q_i = \sum_{k=1}^{7} G_{ik}T_k$.

Note that because our impedance matrices are symmetric, the transfer function matrix is symmetric. Human joint impedance is roughly symmetric; inertia is symmetric by definition [20], and many studies have shown joint stiffness to be nearly symmetric [16, 26, 38]. In our model, I, D, and K are perfectly symmetric, so Z is symmetric, and consequently G as well (the inverse of a symmetric matrix is symmetric). Therefore, $G_{ik} = G_{ki}$, or $\frac{Q_{i/k}(s)}{\mathrm{T}_k(s)} = \frac{Q_{k/i}(s)}{\mathrm{T}_i(s)}$. If the inputs are equal, $q_{i/k}(t) = q_{k/i}(t)$. In other words, the response in DOF i to an input in DOF k is the same as the response in DOF k to an equal input in DOF i. As a corollary, the responses in all DOF due to an input in DOF i are the same as the individual responses in DOF i due to equal inputs in all DOF.

Frequency Response—According to basic linear systems theory [37], if the inputs are sinusoidal, the relationships between inputs and outputs can be specified in terms of magnitude ratios and phase shifts. If the input in DOF k is $\tau_k(t) = A_k \sin(\omega_k t + \phi_k)$, it can be shown [37] that the steady-state output in DOF i is also sinusoidal: $q_{i/k}(t) = M_{ik}A_k\sin(\omega_k t + \phi_k + \phi_{ik})$, with the same frequency (ω_k) but amplitude $M_{ik}A_k$ and phase shift ϕ_{ik} relative to the input. M_{ik} is the ratio of the output magnitude over the input magnitude (called magnitude ratio) and can be calculated from the transfer function as a function of the input frequency: $M_{ik}(\omega_k) = |G_{ik}(j\omega_k)|$, where $j = \sqrt{-1}$. Likewise, the phase shift ϕ_{ik} can be computed from the transfer function as a function of the input frequency: $\phi_{ik}(\omega_k) = \angle G_{ik}(j\omega_k)$ [37]. The total output in DOF i is a linear combination of the individual outputs:

$$q_i(t) = \sum_{k=1}^{7} M_{ik}A_k \sin(\omega_k t + \phi_k + \phi_{ik})$$ [32].

If the sinusoidal inputs are equal, the relationships between inputs and outputs can be specified in terms of a single magnitude ratio and phase shift. To simplify and place all DOF on equal footing (see Discussion), we assumed equal input torques in all DOF: $\tau_k(t) = A$

sin(ωt) for all k. The output then becomes $q_i(t) = A\sum_{k=1}^{7} M_{ik}\sin(\omega t + \omega_{ik})$, which is itself a sinusoid: $q_i(t) = AM_i \sin(\omega t + \phi_i)$. The magnitude ratio M_i and phase shift ϕ_i can be calculated as the magnitude and direction of the vector sum of the k individual vectors (phasors) of magnitude M_{ik} and direction ϕ_i. In practice, M_i and ϕ_i are more easily calculated from the transfer function matrix as follows. Since all inputs are equal, the expression for Q_i above can be written as $Q_i\left[\sum_{k=1}^{7} G_{ik}\right] T = G_i T$. The magnitude ratio and phase shift can be calculated from G_i as $M_i(\omega) = |G_i(j\omega)|$ and $\phi_i(\omega) = \angle G_i(j\omega)$. Thus the output q_i due to multiple inputs of equal frequency, amplitude, and phase is specified by the magnitude ratio and phase shift of the sum of the transfer functions G_{ik} associated with output i.

Simulation Protocol

To investigate how tremor propagates, we calculated from the transfer function matrix the magnitude ratios and phase shifts of all input-output relationships (see below). This is equivalent to injecting sinusoidal torque inputs into all combinations of DOF, observing the resulting displacement amplitude and phase in each DOF, and calculating from the inputs and outputs the magnitude ratios and phase shifts. To simplify and place all DOF on equal footing, we assumed torque inputs in all DOF had equal frequency and phase (see Discussion).

Using this approach, we investigated the following six questions. 1) Where do tremor frequencies fall on the frequency response of the upper limb? Tremors occur most frequently at frequencies between 4 and 12 Hz [12], which we called the tremor band (see Discussion). As an underdamped low-pass filter, the upper limb passes input torques of low frequency, amplifies torques of intermediate frequency, and reduces torques of high frequency. To understand what it does to input torques in the tremor band, we investigated the frequency response of the upper limb in the tremor band, focusing in particular on 4, 8, and 12 Hz as frequencies representing the tremor band. 2) Does tremor propagate mostly because of inertial, damping, or stiffness coupling? Tremor propagates because the off-diagonal elements of the inertia, damping, and stiffness matrices couple the DOF. Does one of these matrices cause most of the coupling? To answer this question, we ran simulations with and without the diagonal elements of these matrices. 3) Does tremor spread to all DOF, or does it focus in certain DOF? The coupling between DOF spreads the tremor, but the spreading may be narrow or broad (i.e. to few or many DOF, respectively). 4) Does tremor propagation change from proximal to distal? Prior studies have found proximal-distal differences in movement characteristics due to differences in impedance [4, 43]. Do these differences in impedance cause differences in tremor propagation as well?

Prior experimental studies have investigated the effect of increasing impedance on tremor [1, 17, 19, 24, 25, 34, 36]. We simulated these effects with the following questions. 5) How does inertial loading affect tremor propagation? We simulated inertial loading by scaling the entire inertia matrix by a factor ranging from 1.0 to 3.0, in increments of 0.2. 6) How does viscoelastic loading affect tremor propagation? Increasing the viscoelasticity of the limb can occur through bracing or muscle contraction. Bracing the upper limb may increase stiffness,

damping, or both. Common commercially available wrist braces increase wrist stiffness by a factor of roughly 1.8 [44], but custom-made braces could be significantly stiffer. To represent a range of possible braces, we increased only stiffness, only damping, and both stiffness and damping, all by factors ranging from 1.0 to 10.0, in increments of 0.5. Muscle contraction increases stiffness in proportion to muscle torque, but it increases damping in proportion to the square root of muscle torque, leaving the damping ratio approximately constant [21, 41]. We simulated co-contraction by increasing the stiffness matrix by a factor of 1-10 (in increments of 0.5) and the damping matrix by the square root of that factor. Prior measurements of stiffness in wrist flexion-extension during torque production have found that a 1-10 increase in stiffness are associated with torques from 0 to 2.1 Nm [10, 11, 28], which is about 27% of the maximum voluntary torque in wrist FE [5].

Data Processing & Analysis

To calculate the magnitude ratios and phase shifts for all input-output combinations, we first transformed our model ($I\ddot{\boldsymbol{q}} + D\dot{\boldsymbol{q}} + K\boldsymbol{q} = \boldsymbol{\tau}$) into state space form [37]:

$$\dot{\boldsymbol{x}}=A_s\boldsymbol{x}+B_s\boldsymbol{\tau} \text{ and } \boldsymbol{y}=C_s\boldsymbol{x}+D_s\boldsymbol{\tau},$$
$$\text{where } \boldsymbol{x}=\begin{bmatrix} \boldsymbol{q} \\ \dot{\boldsymbol{q}} \end{bmatrix}, A_s=\begin{bmatrix} F & E \\ -I^{-1}K & -I^{-1}D \end{bmatrix}, B_s=\begin{bmatrix} F \\ I^{-1} \end{bmatrix}, C_s=\begin{bmatrix} E & F \end{bmatrix}, \text{ and } D_s=F.$$

E and F are 7-by-7 identity and zero matrices, respectively. We implemented this state-space model in Matlab using the *ss* function: *sys_ss* = *ss*(A_s, B_s, C_s, D_s). We then used the *tf* function to derive the transfer function matrix: G = *tf*(*sys_ss*). Finally, we determined the magnitude ratios and phase shifts from G using the *bode* function. Magnitude ratio and phase shift were plotted as functions of frequency. Please note that the magnitude ratio vs. frequency plot is not a power spectrum plot of the tremor; rather, it demonstrates how the limb filters (attenuates, passes, or amplifies) joint torque at each frequency. As stated above, the denominator of each transfer function is a 14th order polynomial in the Laplace variable s, indicating that our system has 14 poles. The system is underdamped; there are 7 pairs of complex poles, each with a natural frequency and damping ratio. Note that these natural frequencies and damping ratios belong to the system as a whole and cannot be assigned to individual DOF. The natural frequencies and damping ratios of the system were determined from G using Matlab's *damp* function. The resonance frequency of each pole was calculated as $\omega_r=\omega_n\sqrt{1-2\zeta^2}$, where ω_n and ζ represent the natural frequency and damping ratio associated with that pole. [37]

Sensitivity Analysis

To determine the effect of uncertainty in our model parameters and test the robustness of our results, we repeated the simulations with variations in inertia, damping, and stiffness. First, we tested inertia, damping, and stiffness matrices at half and twice their original values, scaled individually and in combinations. Second, we tested the sensitivity of our results to individual matrix elements by calculating at 4, 8, and 12 Hz the slope of the magnitude ratio with respect to each element of each impedance matrix. The slope was computed as the

difference derivative from 0.9 to 1.1 times the original value of the matrix element. We identified the most sensitive matrix elements as those with a slope magnitude greater than 0.1 (meaning that multiplying or dividing this matrix element by x increased or decreased the magnitude ratio by $0.1x$ or more), and we repeated simulations at half and twice the original value of these individual matrix elements. Third, we replaced the unknown off-diagonal values of the stiffness matrix (initially assumed zero) with values ranging from small (0.01) to very large (the average of the two corresponding diagonal values), including both positive and negative versions of these values. Since the off-diagonal values of the stiffness matrix are usually considerably smaller than the diagonal values, this range in off-diagonal values is likely larger than the actual range. The damping matrix was calculated by scaling the stiffness matrix, as described above. To determine the off-diagonal values of the damping matrix that did not belong to the shoulder-elbow system or the forearm-wrist system, we scaled using an average of the two constants of proportionality. Fourth, to ensure that any proximal-distal differences were not caused by calculating the damping matrix using different constants of proportionality for the shoulder-elbow and forearm-wrist systems, we repeated our simulations using only one constant (either 0.07 or 0.028) for the whole matrix.

To determine the effect of posture on our results, we also repeated our simulations at a variety of postures (Figure 1). Changes in posture only affected the inertia matrix. Adjustments to the inertia matrix were calculated by adjusting the DH parameter joint angle values (θ) of each DOF for each posture (Table 2). The stiffness and damping matrices were modeled as posture-independent since past measurements of postural stiffness have found short-range stiffness to be largely independent of joint angle [27, 40]. The postures in Figure 1 were chosen as a sample of the most common postures encountered in activities of daily living. We deliberately avoided postures near the limit of the range of motion, where stiffness and damping change significantly. At each posture, we also tested neighboring postures by varying the angle of each DOF through a range of ±15°.

Results

Simulations

Findings are presented as answers to the six questions posed above (Simulation Protocol).

Where do tremor frequencies fall on the frequency response of the upper limb?—The full, coupled 7-DOF system can be characterized by its natural frequencies, damping ratios, and resonance frequencies (which belong to the system as a whole and cannot be assigned to individual DOF). The natural frequencies lay below or in the tremor band: 0.67, 1.08, 1.63, 1.90, 3.22, 4.77, and 6.98 Hz. The associated damping ratios (listed in the same order) were 0.15, 0.24, 0.31, 0.40, 0.29, 0.56, and 0.68 (the range mentioned in Methods refers to the damping ratios of individual DOF in isolation, similar to how they were measured). All damping ratios were below $1/\sqrt{2}$, resulting in resonance at the following frequencies (also listed in the same order): 0.65, 1.02, 1.46, 1.57, 2.94, 2.90, and 1.75 Hz. Due to superposition and some relatively high damping ratios (0.56 and 0.68), Figure 3A exhibits clearly identifiable peaks at only some of these frequencies.

Note that most of the changes in magnitude ratio between DOF occurred at frequencies below the tremor band. Although the magnitude ratio continues to change in the tremor band, lines rarely cross in the tremor band, indicating that the order of output magnitudes is stable in the tremor band. In other words, statements about which DOF have the greatest magnitude ratios are relatively robust for any frequency in the tremor band. How the individual responses combine in a given DOF depends on the phase shift (Figure 3B) as well, since responses may add constructively or destructively (Figure 3C).

Does tremor propagate mostly because of inertial, damping, or stiffness coupling?—Most of the coupling is inertial—removing the off-diagonal elements of the stiffness and damping matrices only had a minor effect (Figure 3D). Because the coupling is mostly inertial, it is somewhat predictable; DOF with parallel axes are coupled (assuming centers of mass are located off-axis). For example, input in shoulder internal rotation affects wrist flexion-extension because their axes are parallel. However, DOF do not need to have parallel axes to affect each other; input in shoulder adduction produces tremor in shoulder internal rotation and wrist flexion, neither of which have axes parallel to shoulder adduction.

Does tremor spread to all DOF, or does it focus in certain DOF?—Tremor spreads in a relatively narrow manner: an input torque in a given DOF propagates mostly to a small subset of DOF (Figure 3D). Since the transfer matrix is symmetric (see Methods), the converse is also true: inputs in only some DOF significantly affect a given DOF. Consequently, simulations with x inputs are not x times more complicated than the single-input case. In fact, many of the responses are dominated by a single input, so for many DOF the response to inputs in all DOF is almost identical to the response to an input in the dominant DOF.

Does tremor propagation change from proximal to distal?—There is a clear proximal-distal increase in the magnitude ratio (Figure 3D). Inputs in proximal DOF affect distal DOF equally or more (often much more) than proximal DOF. While the magnitude does not necessarily increase from DOF 5 to 7, one of these DOF always has the greatest magnitude ratio. In summary, there is more forward propagation than backward propagation. That said, note two caveats. First, even though there is more forward propagation than backward propagation, a distal input creates a bigger distal response than a proximal input of equal magnitude (compare scales in Figure 3D). Second, a distal input creates a bigger proximal response than a proximal input of equal magnitude. For example, an input in DOF 6 creates a bigger response in DOF 3 than an (equal) input in DOF 3.

How does inertial loading affect tremor propagation?—Increasing inertia produces competing trends (Table 3); it decreases the natural frequency, shifting the magnitude ratio curve to the left, but it also decreases the damping ratio, raising the resonance peaks (Figure 4A). The end effect depends on frequency, but in the tremor band it usually decreases the magnitude ratio.

How does viscoelastic loading affect tremor propagation?—Increasing the damping, stiffness, or stiffness and damping together either decreased or increased the magnitude ratio, depending on the amount of increase and the tremor frequency (Table 3).

Because increasing damping alone increased the damping ratio but had no effect on the natural frequency, it always decreased the magnitude ratio (Figure 4B). Increasing stiffness alone increased the natural frequency and decreased the damping ratio, shifting higher resonance peaks toward or into the tremor band, which raised the magnitude ratio (Figure 4C). However, increasing stiffness also decreased the DC-gain, which lowered the magnitude ratio. The end effect depended on the amount of increase in stiffness and the tremor frequency. Increasing both damping and stiffness by the same factor almost always decreased the magnitude ratio in the tremor band, especially for factors greater than 2.5 (Figure 4D). Likewise, increasing stiffness more than damping (by a factor and the square root of the factor, respectively, similar to co-contraction) usually decreased the magnitude ratio, but less robustly than increasing stiffness and damping by the same factor.

Sensitivity Analysis

Errors in inertia, damping, and stiffness produce errors in the exact magnitude ratios, but the pattern of propagation remains relatively unchanged (Figure 5A-C). Multiplying inertia, damping, or stiffness matrices by factors ranging from 0.5 to 2 can have large effects on the magnitude ratios in individual DOF (as described above). However, for frequencies in the tremor band, the relative size of the magnitude ratios is quite unaffected. In particular, the statement that the three distal DOF exhibited the greatest magnitude ratios remained valid. The same is true for errors in the most sensitive elements of the matrices (I_{55}, D_{55}, K_{55}, D_{66}, K_{66}, I_{66}, K_{77}, D_{77} all at 4 Hz). Multiplying these elements by 0.5 or 2 did not significantly alter the results because they affect the three distal DOF (5-7), each of which is dominated by a single phasor. Likewise, replacing the unknown off-diagonal values of the stiffness matrix (initially assumed zero) by non-zero values changed the magnitude ratios but not the pattern of coupling (Figure 5D). Finally, calculating the entire damping matrix using a single constant of proportionality did not significantly change the propagation pattern.

Changing postures affected the coupling between DOF but not the proximal-distal increase in magnitude ratio (Figure 5E). Because coupling is mostly inertial, and because the inertia matrix is a function of posture, the coupling pattern greatly depends on posture. For example, in posture 1, DOF 4 and 7 have parallel axes and are therefore coupled, but pronating the forearm by 90° rotates the axes of DOF 6 and 7 in a way that couples DOF 4 and 6 (instead of 4 and 7). The changes between postures 1-4 did not involve rotations of exactly 90°, so coupling did not generally shift completely from one DOF to another. Nevertheless, the changes were large enough to significantly change the coupling pattern. That said, changes in posture that uncoupled some DOF usually coupled others, resulting in relatively little change in the total response in each DOF due to inputs in all DOF. In particular, the proximal-distal increase in magnitude ratio held true for all four postures.

Discussion

Here we present a basic analysis of tremor propagation to inform the future development of tremor suppressing devices. Optimally suppressing tremor requires a knowledge of the origin, propagation, and distribution of tremor throughout the upper limb. We present the first systematic investigation of how tremor propagates between the shoulder and the wrist.

We deliberately implemented a simple model to focus first on the most basic effects. From these effects we have identified the following basic principles describing the propagation of tremor in the upper limb. Note that these principles were observed under specific simulation conditions (see Limitations below), and more research would be required to generalize outside of these conditions.

Principles of Simulated Tremor Propagation

Principle 1: Tremor amplitude is significantly affected by limb mechanics—The mechanical origin of all tremor is recurring muscle activity, which produces recurring joint torque. Although limb mechanics do not originate tremor, they nonetheless play a significant role in shaping the amplitude of the tremor. As explained above, the amplitude of tremor (the output) is the product of the magnitude of the joint torque (the input) and the magnitude ratio. The magnitude ratio, which reflects limb mechanics, determines if the effect of the input torque is attenuated, passed, or amplified. The damping ratios of the upper limb are generally less than $1/\sqrt{2}$ (see also [41, 45]), resulting in resonance [37]. Although according to our model the frequencies of the resonance peaks (0.65-2.94 Hz) were below the tremor band, the effect of resonance extended into the tremor band for some input-output relationships (Figure 3A). In other words, some of the magnitude ratios were larger in the tremor band than they would be without resonance [29, 30]. In summary, the mechanics of the upper limb shape (and in some cases favor) the expression and propagation of tremor.

Principle 2: Tremor propagates mostly because of inertial coupling—Tremor propagates because the off-diagonal elements of the inertia, damping, and stiffness matrices couple the DOF. Most of this coupling is inertial, not viscoelastic; ignoring the off-diagonal elements of the stiffness and damping matrices has a minimal effect on the propagation pattern (Figure 3D). Note that this statement refers specifically to coupling, not whether inertial effects dominate the dynamics in general. To clarify, prior research showed a proximal-distal shift in the dominating impedance: whereas the dynamics of proximal joints (shoulder and elbow) are thought to be dominated by inertial effects, the dynamics of distal joints (wrist and forearm) are dominated by stiffness effects [39]. However, this prior finding referred to the torques required to overcome the inertia, damping, and stiffness in a given DOF, not coupling between DOF. In addition, it referred to voluntary movements, which occupy a lower frequency band (mostly <5 Hz [35]) than tremor (4-12 Hz), where inertial effects play a smaller role.

Principle 3: Tremor spreads narrowly—Although the inertia, damping, and stiffness matrices couple DOF to each other, some DOF are coupled only weakly or not at all. Consequently, input torque in a DOF significantly affects only a relatively small number of DOF. Because the transfer function matrix is symmetric, this also means that the vast majority of the tremor in a given DOF is due to inputs in a relatively small number of DOF (assuming equal input torques in all DOF). As stated in Principle 2, most of this coupling is inertial, which depends on posture—therefore, the pattern of coupling changes with posture (see Sensitivity Analysis).

Principle 4: Given equal amounts of input torque, the distal DOF have the greatest tremor magnitude—There is a clear increase in tremor magnitude from proximal to distal DOF of the upper limb; one of the three distal joints always has the largest magnitude ratio (Figure 3C-D). It appears this whip effect is caused by proximal-distal differences in impedance. Going from proximal to distal, inertia decreases more rapidly than stiffness (Figure 6). This creates a proximal-distal increase in the natural frequency, which pushes the resonance band to higher frequencies, elevating the magnitude ratios in the tremor band. Although the shoulder and elbow can have higher magnitude ratios than the forearm and wrist DOF (Figure 3), their peaks are below the tremor band.

Principle 5: Increasing inertia can decrease or increase tremor—According to our simulations, increasing inertia usually decreases the magnitude ratio in the tremor band (Figure 4A), but not always. Most past experiments investigating inertial loading have measured a decrease in tremor [17, 25], and there exist a number of commercially available products (e.g. weighted utensils) that claim to mitigate tremor through weighting. However, recent studies have found that inertial loading does not always decrease tremor [34, 36], similar to our simulations. Note that these changes in magnitude ratio with inertial loading do not refer to the decrease in tremor frequency that can occur with inertial loading [17]—that phenomenon cannot be replicated by an LTI model with sinusoidal inputs, because in such a model the output frequency is always equal to the input frequency.

Principle 6: Increasing viscoelasticity can decrease or increase tremor—Increasing damping alone always decreased the magnitude ratio (Figure 4B), but increasing stiffness alone decreased or increased the magnitude ratio depending on the increase in stiffness and the frequency of the input (Figure 4C). Increasing stiffness and damping by the same factor almost always decreased tremor (Figure 4D). Therefore, efforts to develop braces (orthoses) that suppress tremor must discern between stiffening schemes that do and those that do not decrease tremor. That said, effective braces could include properly designed increases in stiffness and/or inertia and do not need to rely solely on damping. Increasing stiffness and damping with no change in the damping ratio (similar to co-contraction) also usually decreased tremor. Prior experiments similarly found that voluntary or artificially elicited muscle contractions attenuate the severity of tremor [19, 24].

Robustness of Principles

We focused here on the frequency band between 4 and 12 Hz, which we called the tremor band. Because our investigation is relevant to all types of tremor (see Introduction), we defined this band relatively wide to be inclusive of most types of tremor [13]. How do the principles relate to tremors that occupy only a narrow range of frequencies within the tremor band? Principle 1, which states that the limb mechanics affect the tremor amplitude, is a fundamental property of system dynamics and is true at any frequency. Principle 2 was found to be true at frequencies across the tremor band (not shown). Principles 3 and 4 were derived from the comparison of magnitude ratios between DOF. Although the magnitude ratios often decrease significantly within the tremor band, the relative sizes of the magnitude ratios remains relatively unaffected, as demonstrated by the low number of curves crossing in the tremor band in Figure 3A (as opposed to the high occurrence of crossing at

frequencies below the tremor band). Therefore, principles 3 and 4 are true at any frequency in the tremor band. Principles 5 and 6 explore the effect of increasing inertia or viscoelasticity on the magnitude ratios. Figures 4A and 4C show that increasing inertia or viscoelasticity can increase or decrease the magnitude ratio, depending on the particular tremor frequency and the limb impedance. Therefore, these last two principles serve as a warning that the effect of inertia and viscoelasticity must be evaluated for each specific case. In summary, the principles are reasonably independent of tremor frequency as long as it is between 4 and 12 Hz.

We characterized the relationship between joint torque and joint displacement, but most of the literature describes tremor in terms of acceleration, not displacement. How do the principles relate to acceleration? If $G(s)$ is the transfer function from joint torque to joint displacement (see Methods), then the transfer function from joint torque to joint acceleration is $H(s) = s^2 G(s)$ since differentiating twice with respect to time is equivalent to multiplying by s^2 in the Laplace domain. The magnitude ratio from torque to acceleration is then $|H(j\omega)| = |(j\omega)^2 G(j\omega)| = \omega^2 |G(j\omega)|$. In other words, the magnitude ratio from torque to acceleration is a scaled version of the magnitude ratio from torque to displacement, where the scaling factor increases with frequency. This scaling is independent of DOF, so the relative proportions between DOF remain completely unchanged. In other words, what increases or decreases the amplitude of displacement in a DOF will also increase or decrease the amplitude of acceleration in that DOF. Consequently, all of the principles are as true for acceleration as they are for displacement.

The principles are also robust against physiologically plausible changes in impedance parameters. Although the tremor magnitudes depend on impedance parameters (Principles 6-7), the sensitivity analysis revealed that the principles were quite insensitive to relatively large changes in inertia, damping, or stiffness (Figure 5A-D). Furthermore, while variations in posture can change which DOF are coupled to each other, the principles are robust against the relatively large changes in postures tested here (Figure 5E). In addition, since most DOF have a dominant phasor that is much larger than the others, the principles are insensitive to transmission delays. Rotating the dominant phasor would not significantly change the magnitude of the vector sum, no matter how large the phase shift is.

Limitations

As mentioned above, we deliberately chose a simple model to establish the most basic, first-order effects. Our model is an LTI model of joint dynamics with realistic values of coupled inertia, damping, and stiffness. To analyze tremor propagation, we used the tools of frequency response, which focus on the steady-state response to sinusoidal inputs. We simulated tremor in a variety of postures away from the limits of the limb's range of motion (ROM). Therefore, our model ignores the following effects: non-sinusoidal torque inputs, non-linear dynamics, time-varying impedance parameters, reflexes, gravity, kinetic tremor (tremor during movement), transient responses, and effects that occur close to the end of the ROM (e.g. when the arm is fully extended). Future studies should characterize how these factors affect tremor propagation, especially the basic principles established here.

By approximating joint torques as sinusoidal inputs, the system was constrained to oscillate at the frequencies of the input torques. In reality, joint torques are not perfectly smooth and may result—in addition to oscillations at the input frequency—in transient oscillations at the damped natural frequencies of the system.

For the multiple-input case, we assumed the torque inputs in different DOF had equal amplitude, frequency, and phase. The amplitudes are most likely not equal, but assuming equal amplitudes allows comparison on an equal footing. The assumption of equal frequency is reasonable—there is no evidence of different frequencies in different DOF. Likewise, the assumption of equal phase is reasonable since the effect of delay between DOF is small because most DOF have a dominant phasor.

Our model focuses on tremor propagation through mechanical coupling but ignores propagation that may occur through neural coupling. Such coupling may result from neuronal entrainment via sensory feedback to central oscillatory networks, causing tremor to spread to other DOF, including DOF that are not mechanically coupled. Finally, our principles are based on simulations and were not validated by comparison to experimentally observed tremor propagation patterns. To the best of our knowledge, there do not exist prior measurements of how tremor propagates throughout the upper limb. The availability of in vivo measurements of tremor propagation patterns would allow one to identify elements of actual tremor reproduced by our simple model (and therefore likely caused by one of the first-order effects included in our model), and those that were not reproduced by our simple model (and therefore likely caused by higher-order effects). Unfortunately, directly measuring tremor propagation between joint torque and joint displacement is not currently possible because it would require in vivo measurements of joint torque in each DOF, which are not currently available. However, because muscle activity is easily measured, it should be possible to validate tremor propagation from muscle activity to joint displacement (via joint torque). The model presented here could be expanded to include the transformation from muscle activity to muscle force (excitation-coupling dynamics) and the transformation from muscle force to joint torque, yielding a total model from muscle activity to tremor (joint displacement). Real measurements of muscle activity and tremor throughout the upper limb would provide both the input and output and should allow one to test the validity of the model.

Conclusion

Using a simple model of upper-limb dynamics, we have established six basic principles describing the propagation of tremor in the upper limb. Our principles agree with prior experimental studies investigating the effects of inertial loading and co-contraction on tremor magnitude. The principles were shown to be stable over the frequency band of most tremors and quite robust against many physiologically plausible variations in joint impedance. We expect that these principles will serve as a foundation for more sophisticated models of tremor propagation and for the development of tremor-suppressing devices.

Acknowledgments

SK Charles and AD Davidson received financial support from NIH Grant R15NS087447, Quantitative Characterization of Essential Tremor for Future Tremor Suppression.

References

1. Aisen ML, Arnold A, Baiges I, Maxwell S, Rosen M. The effect of mechanical damping loads on disabling action tremor. Neurol. 1993; 43
2. Anouti A, Koller WC. Tremor disorders. Diagnosis and management. Western journal of medicine. 1995; 162:510. [PubMed: 7618310]
3. Charles SK, Hogan N. Dynamics of wrist rotations. Journal of Biomechanics. 2011; 44:614–621. [PubMed: 21130996]
4. Charles SK, Hogan N. Stiffness, not inertial coupling, determines path curvature of wrist motions. Journal of Neurophysiology. 2012; 107:1230–1240. [PubMed: 22131378]
5. Colacino FM, Rustighi E, Mace BR. Subject-specific musculoskeletal parameters of wrist flexors and extensors estimated by an EMG-driven musculoskeletal model. Medical Engineering & Physics. 2012; 34:531–540. [PubMed: 21937254]
6. Corke P. Robotics. Vision and Control. 2011
7. Corke P. Robotics, Vision and Control: Fundamental Algorithms in MATLAB. Springer. 2011
8. Craig, JJ. Introduction to Robotics. Upper Saddle River, NJ: Pearson Prentice Hall; 2005.
9. de Leva P. Adjustments to Zatsiorsky-Seluyanov's segment inertia parameters. Journal of Biomechanics. 1996; 29:1223–1230. [PubMed: 8872282]
10. De Serres SJ, Milner TE. Wrist muscle activation patterns and stiffness associated with stable and unstable mechanical loads. Experimental Brain Research. 1991; 86:451–458. [PubMed: 1756819]
11. de Vlugt E, van Eesbeek S, Baines P, Hilte J, Meskers CGM, de Groot JH. Short range stiffness elastic limit depends on joint velocity. Journal of Biomechanics. 2011; 44:2106–2112. [PubMed: 21640995]
12. Deuschl G, Bain P, Brin M. Consensus statement of the movement disorder society on tremor. Ad Hoc Scientific Committee Mov Disord. 1998; 13
13. Deuschl G, Bain P, Brin M, Ad Hoc Sci C. Consensus statement of the Movement Disorder Society on tremor. Movement Disorders. 1998; 13:2–23.
14. Dijkstra EJ. Upper limb project. Mechanical EngineeringUniversity of Twente. 2010
15. Dolan JM, Friedman MB, Nagurka ML. Dynamic and Loaded Impedance Components in the Maintenance of Human Arm Posture. Ieee Transactions on Systems Man and Cybernetics. 1993; 23:698–709.
16. Drake WB, Charles SK. Passive Stiffness of Coupled Wrist and Forearm Rotations. Annals of Biomedical Engineering. 2014; 42:1853–1866. [PubMed: 24912766]
17. Elble RJ. Physiologic and Essential Tremor. Neurology. 1986; 36:225–231. [PubMed: 3945394]
18. Elble RJ, Deuschl G. An update on essential tremor. Current Neurology and Neuroscience Reports. 2009; 9:273–277. [PubMed: 19515278]
19. Gallego JÁ, Rocon E, Belda-Lois JM, Pons JL. A neuroprosthesis for tremor management through the control of muscle co-contraction. Journal of NeuroEngineering and Rehabilitation. 2013; 10:1–13. [PubMed: 23336711]
20. Goldstein, H., Poole, C., Safko, J. Classical Mechanics. San Francisco, CA: Addison Wesley; 2002.
21. Gomi H, Osu R. Task-dependent viscoelasticity of human multijoint arm and its spatial characteristics for interaction with environments. Journal of Neuroscience. 1998; 18:8965–8978. [PubMed: 9787002]
22. Halaki M, O'Dwyer N, Cathers I. Systematic nonlinear relations between displacement amplitude and joint mechanics at the human wrist. Journal of Biomechanics. 2006; 39:2171–2182. [PubMed: 16125181]

23. Hellwig B, Haussler S, Schelter B, Lauk M, Guschlbauer B, Timmer J, Lucking CH. Tremor-correlated cortical activity in essential tremor. Lancet. 2001; 357:519–523. [PubMed: 11229671]
24. Heroux ME, Pari G, Norman KE. The effect of contraction intensity on force fluctuations and motor unit entrainment in individuals with essential tremor. Clinical Neurophysiology. 2010; 121:233–239. [PubMed: 20045376]
25. Hewer RL, Cooper R, Morgan MH. An investigation into the value of treating intention tremor by weighting the affected limb. Brain. 1972; 95
26. Hogan N. The Mechanics of Multi-Joint Posture and Movement Control. Biological Cybernetics. 1985; 52:315–331. [PubMed: 4052499]
27. Hu X, Murray WM, Perreault EJ. Muscle short-range stiffness can be used to estimate the endpoint stiffness of the human arm. J Neurophysiol. 2011; 105:1633–1641. [PubMed: 21289133]
28. Klomp A, de Groot JH, de Vlugt E, Meskers CGM, Arendzen JH, van der Helm FCT. Perturbation Amplitude Affects Linearly Estimated Neuromechanical Wrist Joint Properties. Ieee Transactions on Biomedical Engineering. 2014; 61
29. Lakie M, Vernooij C, Osler C, Stevenson A, Scott J, Reynolds R. Increased gravitational force reveals the mechanical, resonant nature of physiological tremor. The Journal of physiology. 2015; 593:4411–4422. [PubMed: 26108915]
30. Lakie M, Vernooij CA, Osborne TM, Reynolds RF. The resonant component of human physiological hand tremor is altered by slow voluntary movements. The Journal of physiology. 2012; 590:2471–2483. [PubMed: 22431335]
31. Lakie M, Walsh EG, Wright GW. Passive wrist movements - thixotropy -measurement of memory time. Journal of Physiology-London. 1984; 346:P6–P6.
32. Levine, WS. The Control Handbook: Control System Fundamentals. CRC Press; 2010.
33. Lipps DB, Baillargeon EM, Ludvig D, Perreault EJ. System Identification of Multidimensional Shoulder Impedance During Volitional Contractions. IFAC-PapersOnLine. 2015; 48:1369–1374.
34. Ma HI, Hwang WJ, Tsai PL, Hsu YW. The effect of eating utensil weight on functional arm movement in people with Parkinson's disease: a controlled clinical trial. Clinical rehabilitation. 2009; 23:1086–1092. [PubMed: 19906764]
35. Mann KA, Werner FW, Palmer AK. Frequency-Spectrum Analysis Of Wrist Motion For Activities Of Daily Living. Journal of Orthopaedic Research. 1989; 7:304–306. [PubMed: 2918428]
36. Meshack RP, Norman KE. A randomized controlled trial of the effects of weights on amplitude and frequency of postural hand tremor in people with Parkinson's disease. Clinical rehabilitation. 2002; 16:481–492. [PubMed: 12194619]
37. Palm, W. System Dynamics. New York, NY: McGraw Hill; 2014.
38. Pando AL, Lee H, Drake WB, Hogan N, Charles SK. Position-Dependent Characterization of Passive Wrist Stiffness. Ieee Transactions on Biomedical Engineering. 2014; 61:2235–2244. [PubMed: 24686225]
39. Peaden AW, Charles SK. Dynamics of wrist and forearm rotations. Journal of Biomechanics. 2014; 47:2779–2785. [PubMed: 24745814]
40. Perreault EJ, Kirsch RF, Crago PE. Effects of voluntary force generation on the elastic components of endpoint stiffness. Experimental Brain Research. 2001; 141:312–323. [PubMed: 11715075]
41. Perreault EJ, Kirsch RF, Crago PE. Multijoint dynamics and postural stability of the human arm. Experimental Brain Research. 2004; 157:507–517. [PubMed: 15112115]
42. Rocon E, Belda-Lois JM, Sanchez-Lacuesta JJ, Pons JL. Pathological tremor management: Modelling, compensatory technology and evaluation. Technology & Disability. 2004; 16:3–18.
43. Salmond L, Davidson A, Charles S. Proximal-distal differences in movement smoothness reflect differences in biomechanics. In review.
44. Seegmiller D, Charles SK. Common wrist orthoses and their effects on the stiffness of wrist rotations. Journal of Rehabilitation Research and Development. In press.
45. Sinkjaer T, Hayashi R. Regulation of wrist stiffness by the stretch reflex. Journal of Biomechanics. 1989; 22:1133–1140. [PubMed: 2625413]
46. Spong, MW., Hutchinson, S., Vidyasagar, M. Robot Modeling and Control. Hoboken, NJ: John Wiley & Sons, Inc; 2006.

47. Tsuji T, Morasso PG, Goto K, Ito K. Human Hand Impedance Characteristics During Maintained Posture. Biological Cybernetics. 1995; 72:475–485. [PubMed: 7612720]

48. Zesiewicz TA, Elble R, Louis ED, Hauser RA, Sullivan KL, Dewey RB, Ondo WG, Gronseth GS, Weiner WJ. Practice parameter: Therapies for essential tremor - Report of the quality standards subcommittee of the American Academy of Neurology. Neurology. 2005; 64:2008–2020. [PubMed: 15972843]

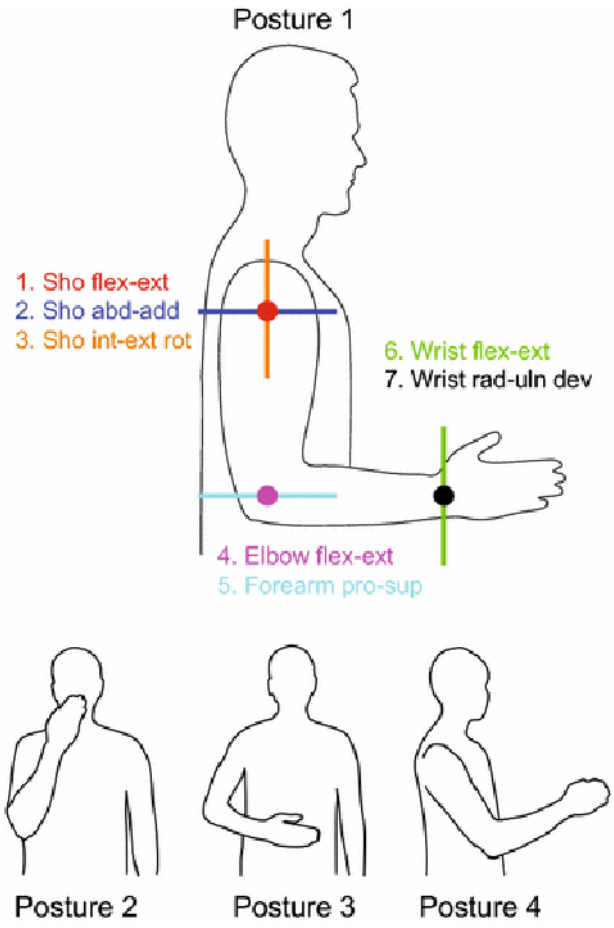

Figure 1.

Degrees of freedom (DOF) and postures included in our study. Our model of the upper limb included seven DOF, designated by their like-colored axes of rotation: Shoulder flexion-extension, shoulder abduction-adduction, shoulder internal-external rotation, elbow flexion-extension, forearm pronation-supination, wrist flexion-extension, and wrist radial-ulnar deviation. Posture 1 is the default posture, and postures 2-4 were used to test the effect of changing posture on tremor propagation. Posture 2 places the hand in front of the mouth and represents feeding and grooming activities. In Posture 3 the hand is in the workspace in front of the abdomen and represents many activities of daily living requiring fine manipulation. Posture 4 represents reaching tasks. Joint angles for each posture are given in Table 2.

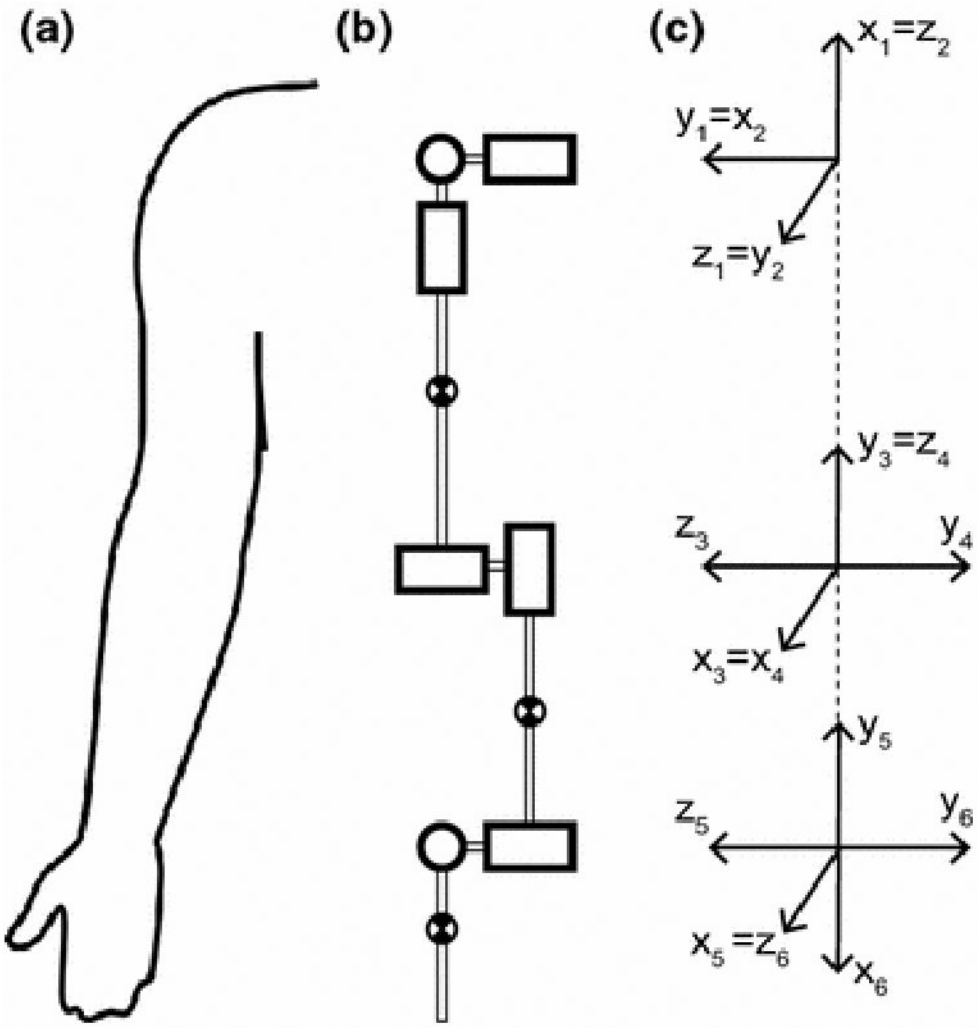

Figure 2.
Kinematic description of the upper limb using the Denavit-Hartenberg (DH) convention. To calculate the full, coupled inertia matrix, we modeled the seven main degrees of freedom of the shoulder, elbow, forearm, and wrist as revolute joints (A-B) and converted the model to DH parameters (Table 2) using the intermediate coordinate frames defined in C. Adapted from [14].

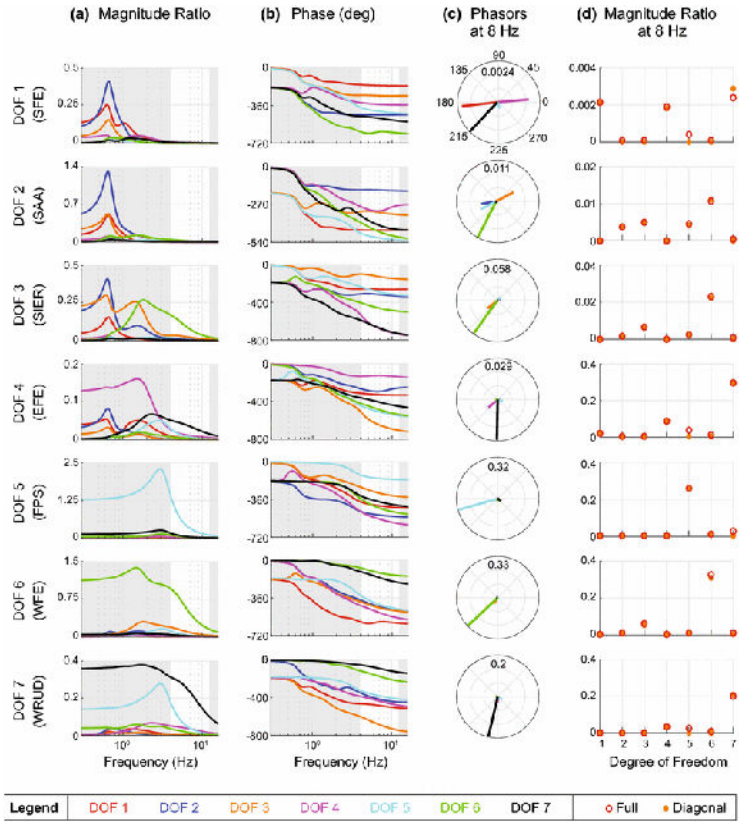

Figure 3.

Frequency response of all input-output relationships. Row presents the frequency response for an input in DOF *i* (row label) and output in DOF *k* (color—see legend). Because the transfer function matrix is symmetric, row *i* also presents the frequency response for an input in DOF *k* (color) and output in DOF *i* (row label). A. Magnitude ratio, i.e. the ratio of the output (tremor) over the input (torque). The tremor band (4-12 Hz) is emphasized in white. B. Phase shift of the output relative to the input. C. Phasor plots for an input frequency of 8 Hz. The magnitude and phase of each phasor is the same as the magnitude ratio and phase shift of the like-colored lines (on the same row), evaluated at 8 Hz. D. Magnitude ratio at 8 Hz vs. DOF. Each plot shows the magnitude ratios for an input in DOF *i* (row label) and output in DOF *k* (x-axis), which is the same as the magnitude ratios for an input in DOF *k* (x-axis) and output in DOF *i* (row label). Red and orange circles were calculated using the full (coupled) and diagonal (uncoupled) stiffness and damping matrices, respectively.

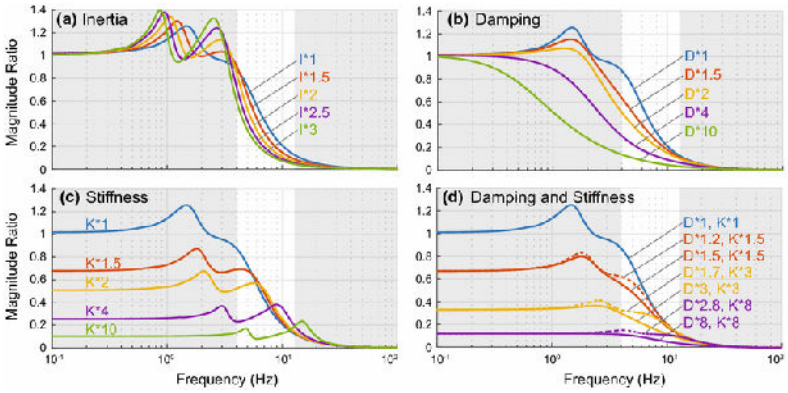

Figure 4.

Effect of inertial and viscoelastic loading on the magnitude ratio, shown here for input and output in DOF 6. The effect of inertial and viscoelastic loading is similar across other input-output relationships. In each plot, the default (no loading) is shown in blue. A. Increasing inertia usually decreases the magnitude ratio in the tremor band, though it can sometimes increase the magnitude ratio, especially at the lower bound of the tremor band. B. Increasing damping alone always decreases the magnitude ratio. C. Increasing stiffness alone can decrease or increase the magnitude ratio depending on the increase in stiffness and the input frequency. D. Increasing stiffness and damping by the same factor (solid lines), or stiffness more than damping (damping by the square root of the factor, dashed lines), usually decreases the magnitude ratio, but can increase the magnitude ratio for some factors and input frequencies.

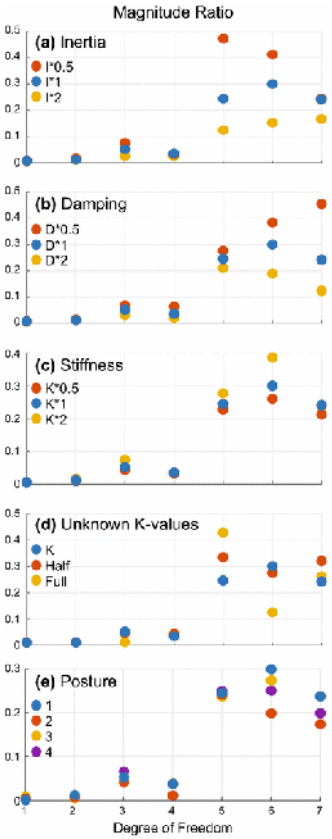

Figure 5.

Sensitivity analysis results shown for the full multi-input–multi-output case (magnitude ratio of the total output in each DOF for equal inputs in *all* DOF). Although changing inertia, damping, stiffness, or posture affects the sizes of the magnitude ratios, the principles presented in the Discussion remain valid. Magnitude ratios were evaluated at 8 Hz. The blue magnitude ratios in each plot were calculated using the default inertia, damping, and stiffness matrices. A-C. Effect of multiplying inertia, damping, or stiffness by factors of 0.5 and 2 on the magnitude ratio. D. Effect of replacing the unknown off-diagonal values in the stiffness matrix (initially assumed zero) by half or the full average of the two corresponding diagonal values. E. Effect of posture. Changing posture tends to switch which DOF are coupled to each other (not shown), but the total amount of coupling in each DOF remains relatively unaffected (assuming inputs in all DOF).

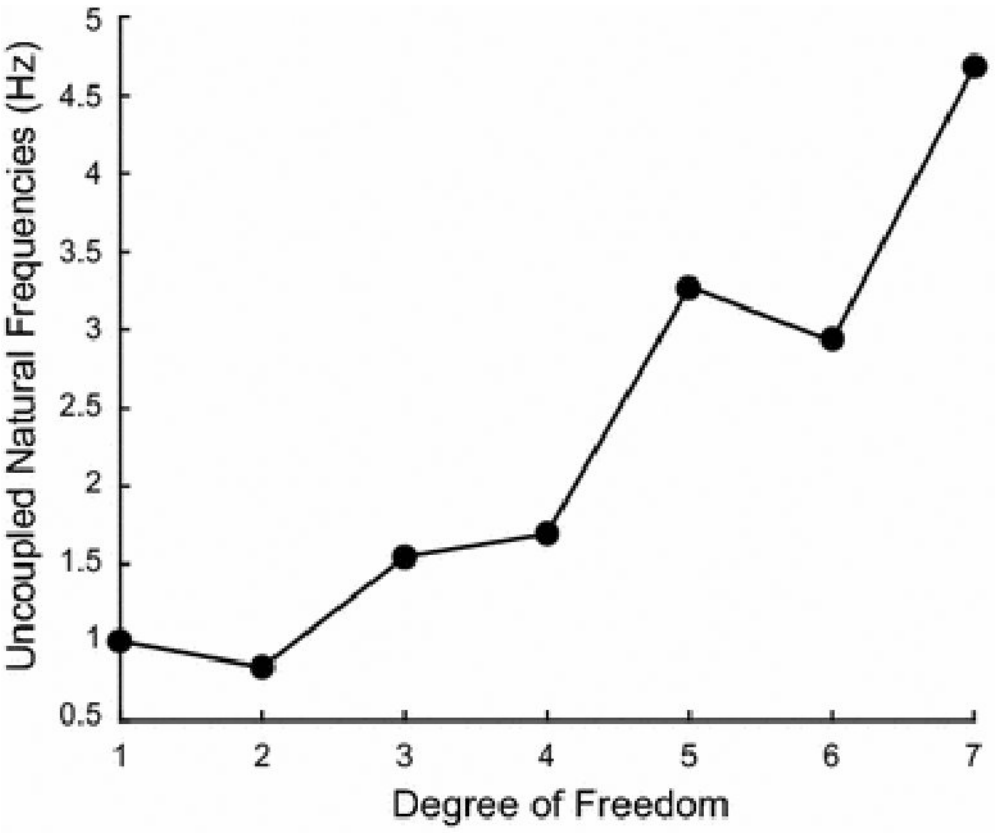

Figure 6.
Uncoupled natural frequency at each DOF. These natural frequencies are proportional to the square root of stiffness over inertia. The proximal-distal increase in natural frequency demonstrates that the proximal-distal decrease in inertia is greater than the decrease in stiffness.

Table 1

Joint inertia, damping, and stiffness matrices used for basic simulations involving posture 1 (other values were tested in the sensitivity analysis). For each matrix, element *ij* (row, column) represents the change in torque in DOF *i* associated with a change in acceleration, velocity, or position (for inertia, damping, or stiffness, respectively) in DOF *j*. The abbreviations represent shoulder flexion-extension (SFE), shoulder abduction-adduction (SAA), shoulder internal-external rotation (SEIR), elbow flexion-extension (EFE), forearm pronation-supination (FPS), wrist flexion-extension (WFE), and wrist radial-ulnar deviation (WRUD).

		SFE	SAA	SIER	EFE	FPS	WFE	WRUD
Inertia (kg m2)	SFE	0.269	0	0	0.076	0	0	-0.014
	SAA	0	0.196	0.083	0	-0.002	0.009	0
	SIER	0	0.083	0.079	0	0	0.011	0
	EFE	0.076	0	0	0.076	0	0	-0.012
	FPS	0	-0.002	0	0	0.002	0	0
	WFE	0	0.009	0.011	0	0	0.003	0
	WRUD	-0.014	0	0	-0.012	0	0	0.003

		SFE	SAA	SIER	EFE	FPS	WFE	WRUD
Damping (Nms/rad)	SFE	0.756	0.184	0.020	0.187	0	0	0
	SAA	0.184	0.383	0.267	0	0	0	0
	SIER	0.020	0.267	0.524	0	0	0	0
	EFE	0.187	0	0	0.607	0	0	0
	FPS	0	0	0	0	0.021	0.001	0.008
	WFE	0	0	0	0	0.001	0.028	-0.003
	WRUD	0	0	0	0	0.008	-0.003	0.082

		SFE	SAA	SIER	EFE	FPS	WFE	WRUD
Stiffness (Nm/rad)	SFE	10.80	2.626	0.279	2.670	0	0	0
	SAA	2.626	5.468	3.821	0	0	0	0
	SIER	0.279	3.821	7.486	0	0	0	0
	EFE	2.670	0	0	8.670	0	0	0
	FPS	0	0	0	0	0.756	0.018	0.291
	WFE	0	0	0	0	0.018	0.992	-0.099

WRUD	0	0	0	0	0.291	-0.099	2.920

Table 2

DH parameters for each posture. Together with Figure 2C, the angle value (θ_i), link offset (d_i), link length (a_i), and link twist (α_i) fully define each posture. Parameters L_{ua}, L_{fa}, and L_h refer to the lengths of the upper arm, forearm, and hand, respectively.

	DH Parameters			
	θ_i	d_i	a_i	α_i
Link 1	$\theta_1 - \pi/2$	0	0	$\pi/2$
Link 2	$\theta_1 + \pi/2$	0	0	$\pi/2$
Link 3	$\theta_1 + \pi/2$	$-L_{ua}$	0	$\pi/2$
Link 4	θ_4	0	0	$-\pi/2$
Link 5	θ_5	$-Lf_a$	0	$\pi/2$
Link 6	$\theta_6 - \pi/2$	0	0	$-\pi/2$
Link 7	θ_7	0	$-L_n$	0

	Posture 1	Posture 2	Posture 3	Posture 4
θ_1	0	$\pi/4$	$\pi/8$	$\pi/8$
θ_2	0	0	0	0
θ_3	0	$\pi/4$	$\pi/4$	$\pi/4$
θ_4	$\pi/2$	$3\pi/4$	$\pi/2$	$\pi/4$
θ_5	$\pi/2$	$\pi/4$	$\pi/4$	$\pi/4$
θ_6	0	$\pi/4$	$\pi/4$	$\pi/4$
θ_7	0	$-\pi/8$	$-\pi/8$	$-\pi/8$

Table 3

Trends illustrating the effects of inertial and viscoelastic loading on the magnitude ratio. Increasing inertia (I), damping (D), and stiffness (K) directly affects the damping ratios (ζ), natural frequencies (ω_n), and DC gains (magnitude ratios at very low input frequencies). Increasing the damping ratios, natural frequencies, and DC gains alone generally decreases, increases, and decreases, respectively, the magnitude ratios. The combination of these competing effects dictate whether the magnitude ratio in the tremor band ($M_{4–12\ Hz}$) increases (↑), decreases (↓), or does either depending on the amount of increase and the input frequency (↑↓). "Stiffness and Damping" refers to increasing both by the same factor, whereas "Co-contraction" refers to increasing stiffness by a factor and damping by the square root of that factor, similar to what occurs in co-contraction.

Simulation	I	D	K	ζ	ω_n	*DC gain*	$M_{4–12\ Hz}$
Inertia	↑	–	–	↓	↓	–	↑↓
Damping	–	↑	–	↑	–	–	↓
Stiffness	–	–	↑	↓	↑	↓	↑↓
Stiffness and Damping	–	↑	↑	↑	↑	↓	↑↓
Co-contraction	–	↑	↑	–	↑	↓	↑↓